PLOS COMPUTATIONAL BIOLOGY

RESEARCH ARTICLE

Beyond homogeneity: Assessing the validity of the Michaelis–Menten rate law in spatially heterogeneous environments

Seolah Shin[1,2☯], **Seok Joo Chae**[2,3☯], **Seunggyu Lee**[2,4*], **Jae Kyoung Kim**[2,3*]

1 Department of Applied Mathematics, Korea University, Sejong, Republic of Korea, **2** Biomedical Mathematics Group, Pioneer Research Center for Mathematical and Computational Sciences, Institute for Basic Science, Daejeon, Republic of Korea, **3** Department of Mathematical Sciences, KAIST, Daejeon, Republic of Korea, **4** Division of Applied Mathematical Sciences, Korea University, Sejong, Republic of Korea

☯ These authors contributed equally to this work.
* s.lee:sky509@korea.ac.kr (SL); jk.kim:jaekkim@kaist.ac.kr (JKK)

Citation: Shin S, Chae SJ, Lee S, Kim JK (2024) Beyond homogeneity: Assessing the validity of the Michaelis–Menten rate law in spatially heterogeneous environments. PLoS Comput Biol 20(6): e1012205. https://doi.org/10.1371/journal.pcbi.1012205

Editor: Andrea Ciliberto, IFOM - the Firc Insitute of Molecular Oncology, ITALY

Received: January 26, 2024

Accepted: May 24, 2024

Published: June 6, 2024

Data Availability Statement: All experimental data and computational code are publicly available on GitHub, at https://github.com/Mathbiomed/PDE_QSSA.

Funding: This work was supported by the Institute for Basic Science (grant no. IBS-R029-C3 to JKK), and the National Research Foundation of Korea (NRF) grant funded by the Korea government (MSIP) (grant no. RS-2024-00342949 to SL), and Regional Innovation Strategy (RIS) through the NRF funded by the Ministry of Education (MOE)

Abstract

The Michaelis–Menten (MM) rate law has been a fundamental tool in describing enzyme-catalyzed reactions for over a century. When substrates and enzymes are homogeneously distributed, the validity of the MM rate law can be easily assessed based on relative concentrations: the substrate is in large excess over the enzyme-substrate complex. However, the applicability of this conventional criterion remains unclear when species exhibit spatial heterogeneity, a prevailing scenario in biological systems. Here, we explore the MM rate law's applicability under spatial heterogeneity by using partial differential equations. In this study, molecules diffuse very slowly, allowing them to locally reach quasi-steady states. We find that the conventional criterion for the validity of the MM rate law cannot be readily extended to heterogeneous environments solely through spatial averages of molecular concentrations. That is, even when the conventional criterion for the spatial averages is satisfied, the MM rate law fails to capture the enzyme catalytic rate under spatial heterogeneity. In contrast, a slightly modified form of the MM rate law, based on the total quasi-steady state approximation (tQSSA), is accurate. Specifically, the tQSSA-based modified form, but not the original MM rate law, accurately predicts the drug clearance via cytochrome P450 enzymes and the ultrasensitive phosphorylation in heterogeneous environments. Our findings shed light on how to simplify spatiotemporal models for enzyme-catalyzed reactions in the right context, ensuring accurate conclusions and avoiding misinterpretations in *in silico* simulations.

Author summary

For over a century, scientists have relied on the simple Michaelis–Menten (MM) rate law to explain how enzymes function. The conventional criterion for using the MM rate law has been derived in homogeneous environments where species are evenly dispersed (e.g., *in vitro* experiments). Here, we found that the conventional criterion does not work in

(grant no. 2021RIS-004 to SL). The funders had no role in study design, data collection and analysis, decision to publish, or preparation of the manuscript.

Competing interests: The authors have declared that no competing interests exist.

intracellular environments where species are heterogeneously distributed and diffuse slowly. However, we find that a slightly modified formula of the MM rate law, based on total quasi-steady state approximation (tQSSA), is accurate even in heterogeneous environments. In particular, this modified formula, unlike the MM rate law, accurately predicts the rate of drug metabolism and ultrasensitive phosphorylation when species are not evenly distributed. Our results provide insight into how to use simplified models for describing enzyme functions in such non-evenly distributed environments.

Introduction

Enzymes play significant roles in regulating the rates of reactions in living organisms, influencing essential processes such as metabolism, signal transduction, and cellular regulation [1–4]. For over a century, the Michaelis–Menten (MM) equation has been the prevailing framework for describing rates of enzyme-catalyzed reactions [5–11]. Specifically, the MM rate law effectively describes the rate of product (P) accumulation in a single enzyme-catalyzed mechanism in terms of substrate concentration (S):

$$\frac{dP}{dt} = k_{cat}\frac{E_T S}{K_M + S}, \tag{1}$$

where k_{cat} is the catalytic constant, and K_M is the MM constant, and E_T is the total enzyme concentration. The MM rate law was proposed by Henri [5] and Michaelis and Menten [6], and derived by Briggs and Haldane using an approach known as the quasi-steady state approximation (QSSA) [7]. This approximation has been referred to as the standard quasi-steady state approximation (sQSSA) [11–14]. The sQSSA has also been utilized to describe a variety of observable biomolecular interactions between genes and transcription factors [15, 16], and receptors and ligands [17, 18].

The MM rate law based on the sQSSA is accurate when the enzyme concentration is low enough to be $E_T \ll S_T + K_M$, where S_T is total substrate and product concentration [11–14], referred to as the validity condition of the sQSSA throughout this study. Since the concentrations of enzyme and substrate are roughly comparable in protein interaction reactions, the sQSSA model can be inaccurate [11, 19]. To resolve this inaccuracy of the sQSSA model, an alternative model based on the total quasi-steady state approximation (tQSSA) was proposed [11, 13, 14, 20–23]. Even when the concentration of enzymes is high, and thus the validity condition of the sQSSA is not satisfied, the tQSSA model is accurate [11, 13, 14, 20–23]. Thus, the tQSSA model has been recognized as a more reliable approximation tool for the enzyme–catalyzed reaction model than the sQSSA model.

Both the sQSSA and the tQSSA models are based on an ordinary differential equation (ODE) that assumes homogeneous distributions of species, including enzymes and substrates. However, this assumption appears not to be valid within the cell, unlike in *in vitro* experimental environments. Specifically, enzymes are localized in particular organelles depending on their type and function. For instance, enzymes managing the respiratory chain and oxygen reduction reactions are highly concentrated in mitochondria [24]. Furthermore, cytochrome P450 (CYP) enzymes, essential for drug metabolism, are located in microsomes in the endoplasmic reticulum (ER) of liver cells [25]. Thus, it would be inaccurate to use an ODE to describe enzyme-catalyzed reactions in cells where the assumption of the homogeneous distribution is violated. Instead, employing a partial differential equation (PDE) that accounts for the spatial distribution of chemical species would be a more valid approach.

Previous studies have shown that the applicability of the sQSSA, and thus the MM rate law, can be extended to PDE when the local concentration can be assessed across the entire spatial domain. Specifically, when $E_T \ll S_T + K_M$ (the validity condition of the sQSSA in ODE) is satisfied at each point within the domain, using the MM rate law in PDE is accurate under various diffusion conditions: (1) when the diffusion time scale is shorter than the fast reaction time scale or longer than the slow reaction time scale [26], (2) when the diffusion time scale aligns with the slow kinetic time scale [27], and (3) when the dissociation of the complex is significantly faster than the diffusion [28]. However, verifying this validity condition necessitates measuring enzyme and substrate concentrations at every point within the entire cell, which is impossible. On the other hand, the spatial average concentrations of enzyme and substrate can be measured using techniques such as western blot [29], UV-Vis spectroscopy [30] and Enzyme-Linked Immunosorbent Assay [31]. This necessitates a validity condition based on spatial average concentrations rather than the local concentration.

Here we investigated whether the sQSSA in PDE is valid when $\bar{E}_T \ll \bar{S}_T + K_M$, where $\bar{E}_T$ and $\bar{S}_T$ are the spatial average of the total enzyme concentration and the total substrate and product concentration across the domain, respectively. Specifically, we showed that the sQSSA in PDE can still be accurate although the spatial averages of molecular concentrations do not satisfy $\bar{E}_T \ll \bar{S}_T + K_M$, when the substrate and the enzyme are localized in different regions and their diffusion is slower than slow reactions. Conversely, we found that the sQSSA in PDE may introduce substantial errors, even if the spatial average concentrations satisfy $\bar{E}_T \ll \bar{S}_T + K_M$, especially when the substrate and the enzyme are localized in the same region under conditions of slow diffusion. As a result, employing the sQSSA model to simulate drug metabolism in the liver, where the CYP enzyme is localized in the ER, leads to considerable error in predicting drug clearance, the rate of a drug's breakdown in the liver. Unlike the sQSSA, using the tQSSA in PDE was accurate for all of these cases because the tQSSA in ODE is generally valid regardless of enzyme concentration. These findings imply that in heterogeneous spaces, where validating the sQSSA at every point is challenging, utilizing the sQSSA in PDE poses a risk. Thus, the tQSSA should be used to model enzyme-catalyzed reactions in heterogeneous spaces.

Results

QSSAs for ODE describing enzyme-catalyzed reactions

An enzyme-catalyzed reaction can be described by the following ODE system based on mass-action kinetics (Fig 1):

$$\begin{aligned} \frac{dS}{dt} &= -k_f S \cdot E + k_b C, \\ \frac{dE}{dt} &= -k_f S \cdot E + k_b C + k_{cat} C, \\ \frac{dC}{dt} &= k_f S \cdot E - k_b C - k_{cat} C, \\ \frac{dP}{dt} &= k_{cat} C, \end{aligned} \tag{2}$$

where E and C are the concentration of the enzyme and the complex, respectively. The enzyme reversibly binds the substrate to form the complex and then the complex irreversibly dissociates into product and enzyme. Note that $E_T \equiv E + C$ and $S_T \equiv S + C + P$ are always conserved. By utilizing conservation laws, this model can be effectively expressed as an ODE system with

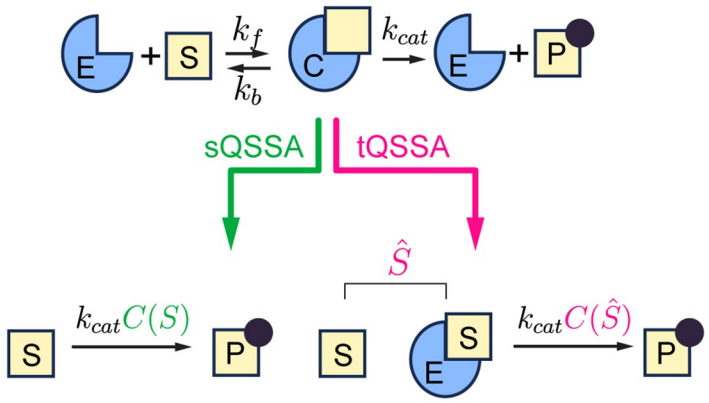

Fig 1. QSSAs for an enzyme-catalyzed reaction. A model describing an enzyme-catalyzed reaction based on mass-action kinetics (Eqs 2 and 9) can be simplified using either the $sQSSA_o$ (Eqs 5 and 11) and the $sQSSA_p$ (Eq 11) or the $tQSSA_o$ (Eq 8) and the $tQSSA_p$ (Eq 13). Both approximations of QSS are defined in terms of S or $\hat{S} = S + C$.

https://doi.org/10.1371/journal.pcbi.1012205.g001

two variables, S and C, as follows:

$$\begin{aligned} \frac{dS}{dt} &= -k_f S \cdot (E_T - C) + k_b C, \\ \frac{dC}{dt} &= k_f S \cdot (E_T - C) - k_b C - k_{cat} C, \end{aligned} \tag{3}$$

where P can be simply obtained by $P = S_T - C - S$. We can further simplify the model by assuming that C reaches a quasi-steady state (QSS) more rapidly than S and then both C and S slowly track along the QSS. The approximation to QSS (i.e., QSSA) can be obtained by solving $dC/dt = 0$:

$$C(S) = \frac{E_T S}{K_M + S}, \tag{4}$$

where $K_M = \frac{k_b + k_{cat}}{k_f}$ is the MM constant. By substituting Eq 4 for Eq 3, the MM rate law can be derived:

$$\frac{dP}{dt} = k_{cat} \frac{E_T S}{K_M + S}. \tag{5}$$

As the MM rate law is derived by using the sQSSA for ODE systems, we refer it to as the $sQSSA_o$ model throughout the study. The $sQSSA_o$ model is accurate when E_T is sufficiently small (i.e., $E_T \ll S_T + K_M$) [11–14]. Thus, when E_T and S_T are comparable, such as in protein interaction reactions, using the $sQSSA_o$ model can lead to significant errors [11, 19]. This inaccuracy arises from treating S as a slow variable, even though S is also affected by fast binding and unbinding reactions [11, 32]. In other words, the time scale of S is not significantly longer than that of C, violating the underlying assumption of the sQSSA.

Such inaccuracy can be resolved by introducing the total substrate concentration $\hat{S} = S + C$. By using $\hat{S}$, Eq 3 can be rewritten as follows:

$$\begin{aligned} \frac{d\hat{S}}{dt} &= -k_{cat}C, \\ \frac{dC}{dt} &= k_f(\hat{S} - C)(E_T - C) - k_bC - k_{cat}C. \end{aligned} \tag{6}$$

As $\hat{S}$ is now solely affected by a slow reaction (i.e., $\frac{d\hat{S}}{dt} = -k_{cat}C$), the time scale of $\hat{S}$ is significantly longer than that of C. Thus, C is more likely to reach QSS before $\hat{S}$ changes appreciably. The QSSA of C given $\hat{S}$ can be obtained by solving $\frac{dC}{dt} = 0$ in Eq 6:

$$C(\hat{S}) = \frac{1}{2}\left[E_T + \hat{S} + K_M - \sqrt{(E_T + \hat{S} + K_M)^2 - 4E_T\hat{S}}\right]. \tag{7}$$

Substituting this QSSA for C (Eq 7) back into the model (Eq 6) results in the reduced model:

$$\frac{dP}{dt} = \frac{1}{2}k_{cat}\left[E_T + \hat{S} + K_M - \sqrt{(E_T + \hat{S} + K_M)^2 - 4E_T\hat{S}}\right], \tag{8}$$

where $\hat{S} = S_T - P$. As this model is derived with the total quasi-steady state approximation for ODE systems [11, 13, 14, 20–23], we referred it to as the tQSSA_o model throughout the study.

It was shown that the tQSSA_o model is accurate when the condition $\frac{K}{2S_T}\frac{E_T+K_M+S_T}{\sqrt{(E_T+K_M+S_T)^2-4E_TS_T}} \ll 1$ is satisfied, where $K = k_{cat}/k_f$. Given that $\frac{K}{2S_T}\frac{E_T+K_M+S_T}{\sqrt{(E_T+K_M+S_T)^2-4E_TS_T}} < \frac{1}{4}$ is always satisfied, it has been believed that the tQSSA_o model is generally accurate [11, 13, 14, 20–23]. In particular, when the concentration of enzymes is high and thus the sQSSA_o model is not valid, the tQSSA_o model is accurate [11, 13, 14, 20–23]. Although Eilertsen and Schnell recently identified conditions where even the tQSSA_o model becomes inaccurate (i.e., the region outside of $\frac{k_{cat}E_T}{k_f(K_M+E_T)^2} \ll 1$) [33], this limitation of the tQSSA_o is confined to a very small region of the parameter space. In particular, even when $S_T/K_M \ll 1$ and thus the above conditions are not satisfied [33], it was also shown that the tQSSA_o model still performs reasonably well. Thus, the tQSSA_o model has been recognized as a reliable approximation tool for the enzyme-catalyzed reaction model [11].

QSSAs for PDE describing enzyme-catalyzed reactions

So far, we have discussed the application of QSSAs in ODE systems, assuming the even distribution of species in space. To incorporate the spatial distribution of species, we can employ the following PDE system [26–28] defined on a bounded region with a smooth boundary Ω:

$$\begin{aligned} \frac{\partial S}{\partial t} &= D_S\Delta S - k_fS\cdot E + k_bC, && \text{in } (0,\ \infty)\times\Omega \\ \frac{\partial E}{\partial t} &= D_E\Delta E - k_fS\cdot E + k_bC + k_{cat}C, && \text{in } (0,\ \infty)\times\Omega \\ \frac{\partial C}{\partial t} &= D_C\Delta C + k_fS\cdot E - k_bC - k_{cat}C, && \text{in } (0,\ \infty)\times\Omega \\ \frac{\partial P}{\partial t} &= D_P\Delta P + k_{cat}C, && \text{in } (0,\ \infty)\times\Omega \end{aligned} \tag{9}$$

where diffusion coefficients of S, E, C, and P are denoted as D_S, D_E, D_C, and D_P, respectively.

In this study, we mainly used a one-dimensional domain $\Omega = (0, L)$, where L is the length of the domain. Besides, we used zero-Neumann boundary conditions and continuous initial conditions (ICs) $S(0, x) = S_0(x)$, $E(0, x) = E_0(x)$, $C(0, x) = C_0(x)$, and $P(0, x) = P_0(x)$.

Analogous to the ODE system, we can express Eq 9 as follows by using $E_T = E + C$:

$$\begin{aligned}
\frac{\partial S}{\partial t} &= D_S \Delta S - k_f S(E_T - C) + k_b C, && \text{in } (0,\infty) \times \Omega \\
\frac{\partial E_T}{\partial t} &= D_E \Delta (E_T - C) + D_C \Delta C, && \text{in } (0,\infty) \times \Omega \\
\frac{\partial C}{\partial t} &= D_C \Delta C + k_f S(E_T - C) - k_b C - k_{cat} C, && \text{in } (0,\infty) \times \Omega \\
\frac{\partial P}{\partial t} &= D_P \Delta P + k_{cat} C, && \text{in } (0,\infty) \times \Omega
\end{aligned} \tag{10}$$

Note that E_T is no longer pointwise conserved because the diffusion can change the concentration of the enzyme. The above PDE system (Eq 10) can be simplified by applying QSSA as in the ODE system when the time scales are separated. Since species not only react but also diffuse throughout the cell, it is essential to compare the diffusion time scale with the reaction time scale. When the diffusion time scale is comparable to or shorter than the fast reaction time scale, the concentrations of each species are rapidly homogenized, resulting in similar dynamics to ODE at each point [26]. Thus, we focused on the situation when the diffusion time scale is comparable to or longer than the slow reaction time scale. Under this condition, C reaches QSS before the concentrations of other species change significantly by diffusion and reaction [27]. Then, by using the sQSSA_o ($C(S) = \frac{E_T S}{S + K_M}$), the PDE model (Eq 10) can be reduced as follows [27]:

$$\begin{aligned}
\frac{\partial S}{\partial t} &= D_S \Delta S - k_{cat} C(S), && \text{in } (0,\infty) \times \Omega \\
\frac{\partial E_T}{\partial t} &= D_E \Delta (E_T - C(S)) + D_C \Delta C(S), && \text{in } (0,\infty) \times \Omega \\
\frac{\partial P}{\partial t} &= D_P \Delta P + k_{cat} C(S), && \text{in } (0,\infty) \times \Omega
\end{aligned} \tag{11}$$

where $C(S) = \frac{E_T S}{S + K_M}$. As the sQSSA_o is used in the PDE system, we refer to this model (Eq 11) as the sQSSA_p.

As in the ODE (Eq 6), we introduce a slow variable $\hat{S} = S + C$ to the PDE system (Eq 10) as follows:

$$\begin{aligned}
\frac{\partial \hat{S}}{\partial t} &= D_S \Delta (\hat{S} - C) + D_C \Delta C - k_{cat} C, && \text{in } (0,\infty) \times \Omega \\
\frac{\partial E_T}{\partial t} &= D_E \Delta (E_T - C) + D_C \Delta C, && \text{in } (0,\infty) \times \Omega \\
\frac{\partial C}{\partial t} &= D_C \Delta C + k_f (\hat{S} - C)(E_T - C) - k_b C - k_{cat} C, && \text{in } (0,\infty) \times \Omega \\
\frac{\partial P}{\partial t} &= D_P \Delta P + k_{cat} C. && \text{in } (0,\infty) \times \Omega
\end{aligned} \tag{12}$$

Then by using the tQSSA$_o$ of $C(\hat{S})$ (Eq 7), we obtained the following reduced PDE system:

$$\begin{aligned}
\frac{\partial \hat{S}}{\partial t} &= D_S\Delta(\hat{S} - C(\hat{S})) + D_C\Delta C(\hat{S}) - k_{cat}C(\hat{S}), && \text{in } (0,\infty)\times\Omega \\
\frac{\partial E_T}{\partial t} &= D_E\Delta(E_T - C(\hat{S})) + D_C\Delta C(\hat{S}), && \text{in } (0,\infty)\times\Omega \\
\frac{\partial P}{\partial t} &= D_P\Delta P + k_{cat}C(\hat{S}), && \text{in } (0,\infty)\times\Omega
\end{aligned} \tag{13}$$

where $C(\hat{S}) = \frac{1}{2}\left[E_T + \hat{S} + K_M - \sqrt{(E_T + \hat{S} + K_M)^2 - 4E_T\hat{S}}\right]$. We refer to this model (Eq 13) as the tQSSA$_p$.

The accuracy of the sQSSA$_p$, but not the tQSSA$_p$ varies depending on whether the environment is homogeneous or heterogeneous

We explored the accuracy of the sQSSA$_p$ (Eq 11) and the tQSSA$_p$ (Eq 13) in both homogeneous and heterogeneous environments, by comparing their behaviors to those of the full model (Eq 9). To simulate these models, we first chose biologically realistic values for the parameters (D_S, D_E, D_C, D_P, k_f, k_b, k_{cat}, and L). For instance, we assigned a diffusion coefficient of $D_* = 0.2\mu m^2/s$ to all species, which is lower than typical protein diffusion coefficients [34] but corresponds to the diffusion coefficient of large-sized proteins (e.g., PER2 protein complex) [35]. Furthermore, since the protein-protein binding occurs with a rate on the order of $10^6 M^{-1}s^{-1}$, often ranging up to $\sim 10^8 M^{-1}s^{-1}$ [36, 37], we have used $k_f = 3.4 \cdot 10^6 M^{-1}s^{-1}$. We set k_b and k_{cat} to $60s^{-1}$ and $3.2s^{-1}$, respectively, ensuring that K_M, k_{cat}, and k_{cat}/K_M are in the range of typical enzyme kinetic parameters [38]. Finally, the length of the domain Ω, L, was set to $30\mu m$, which falls within the human cell size range [39].

We first investigated the homogeneous ICs so that the validity condition of the sQSSA$_o$ ($E_T \ll S_T + K_M$) is satisfied at every point of the domain (Fig 2A). In this case, as expected, both the sQSSA$_p$ and the tQSSA$_p$ accurately capture P of the full model at each point (Fig 2B), and thus the spatial average of P, $\bar{P}$ (Fig 2C).

Next, we made the ICs heterogeneous while maintaining the spatial average concentrations of Fig 2A, so that the spatial average concentrations satisfy the validity condition of the sQSSA$_o$ ($\bar{E}_T \ll \bar{S}_T + K_M$) (Fig 2D). Specifically, we increased the concentrations of S and E near $x = 30\mu m$ and decreased the concentrations in other regions. As a result, the validity condition of the sQSSA$_o$ ($S_T + K_M \approx E_T$) is not satisfied near $x = 30\mu m$ (Fig 2D). In this region, the sQSSA$_p$ overestimates P of the full model (Fig 2E). Since the majority of S is localized at this invalid region, the majority of P is generated in that region, and thus, the sQSSA$_p$ also overestimates $\bar{P}$ compared to the full model (Fig 2F). On the other hand, even with these heterogeneous ICs, the tQSSA$_p$ accurately simulates P (Fig 2E and 2F).

The impact of a heterogeneous environment on the accuracy of the sQSSA$_p$ may diminish with faster diffusion because the initial spatial distribution of species is homogenized and the spatial averages of the concentrations satisfy the validity of the sQSSA$_o$ (Fig 2A). Indeed, as the diffusion coefficient (D_*) increases, the accuracy of the sQSSA$_p$ becomes accurate (S1 Fig). Specifically, when the diffusion time scale (L^2/D_*) is comparable to the time scale of the slowest reaction ($1/k_{cat}$), the sQSSA$_p$ accurately captures the behavior of the full model. On the other hand, when the diffusion time scale is $\sim$100-fold slower than the time scale of the slowest reaction, the sQSSA$_p$ is inaccurate. Taken together, the inaccuracy of the sQSSA$_p$ arises when the diffusion is slower than all of the reactions.

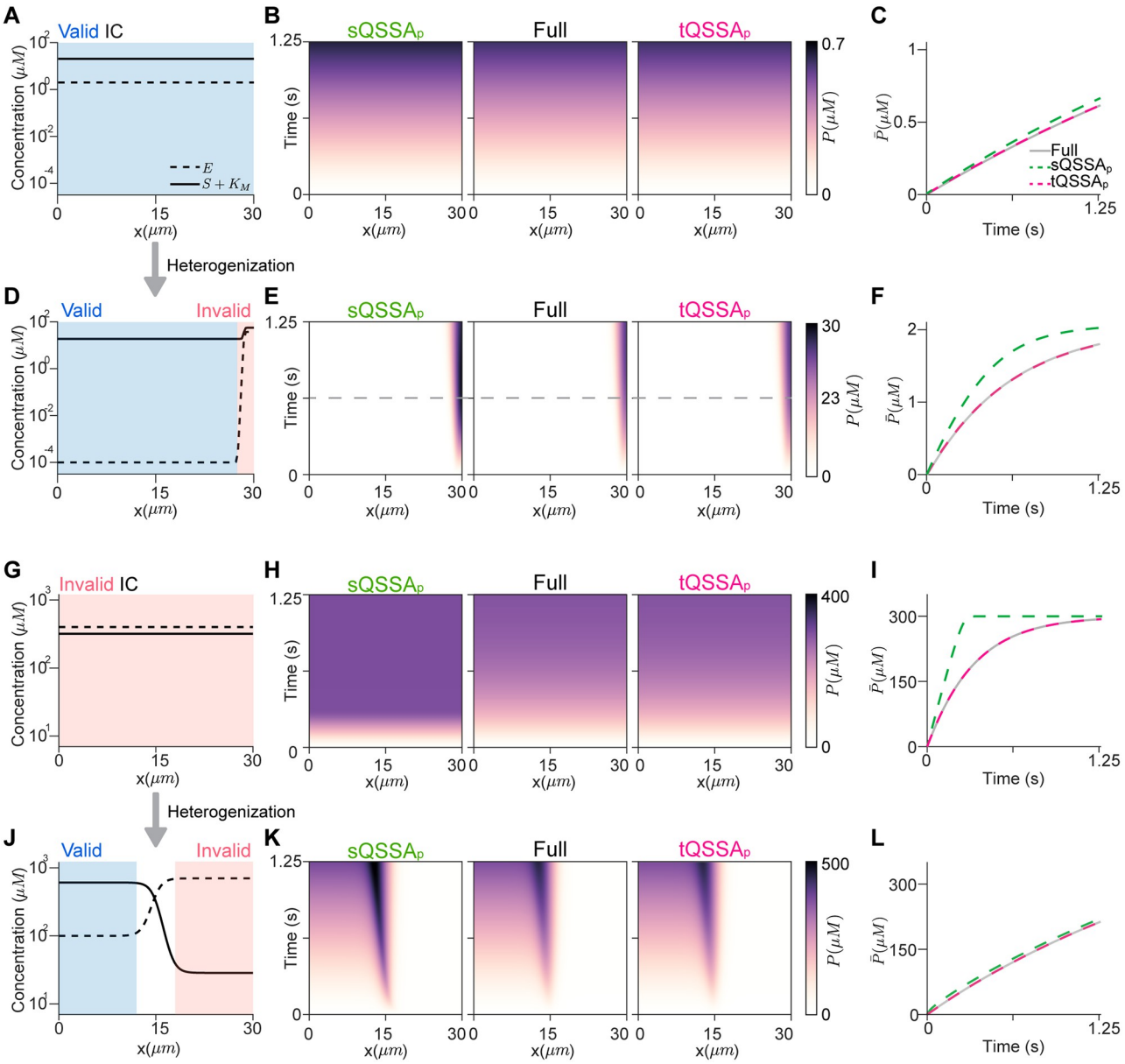

Fig 2. The accuracy of the sQSSA$_p$ and the tQSSA$_p$ in heterogeneous environments. (A) Homogeneous ICs that satisfy the validity condition of the sQSSA$_o$ throughout the domain (blue region). $E_0 \equiv 2\mu M$, $S_0 \equiv 2\mu M$ and $K_M = 18.5\mu M$. **(B-C)** Both the sQSSA$_p$ and the tQSSA$_p$ accurately capture the production of P throughout the domain (B) and the spatial average $\bar{P}$ (C). **(D)** The ICs in (A) were heterogenized so that the validity condition of the sQSSA$_o$ model does not hold near $x = 30\mu m$ (red region), unlike the other region (blue region). Here, $E_0(x) = S_0(x) = 18.5(\tanh(20x/3 - 190) + 1) + 10^{-4}\mu M$, which maintain the spatial average concentration with the ICs in (A), was used. **(E-F)** The tQSSA$_p$ model, but not the sQSSA$_p$ model, is accurate. **(G)** The homogeneous ICs that do not satisfy the validity condition of the sQSSA$_o$ through the domain. Here, $E_0 \equiv 400\mu M$, $S_0 \equiv 300\mu M$, and $K_M = 18.5\mu M$. **(H-I)** The tQSSA$_p$ model, but not the sQSSA$_p$ model, is accurate. **(J)** The ICs in (G) were heterogenized so that the validity condition of the sQSSA$_o$ is satisfied in $x < 15\mu m$ (blue region), but not in $x \geq 15\mu m$ (red region). Here, $E_0(x) = 300(\tanh(2x/3 - 10) + 1) + 100\mu M$ and $S_0(x) = 290(\tanh(10 - 2x/3) + 1) + 10\mu M$, which keep the spatial average concentration with the ICs in (G), were used. **(K-L)** Both the sQSSA$_p$ and tQSSA$_p$ models are accurate. For all simulations, $C_0 \equiv 0\mu M$, $P_0 \equiv 0\mu M$ and $k_f = 3.4 \cdot 10^6 M^{-1}s^{-1}$, $k_b = 60s^{-1}$, $k_{cat} = 3.2s^{-1}$, $D_E = D_S = D_C = D_P = D_* = 0.2\mu m^2/s$.

https://doi.org/10.1371/journal.pcbi.1012205.g002

We next investigated the opposite case: can the $sQSSA_p$ be accurate, even if $\bar{E}_T \ll \bar{S}_T + K_M$ is not satisfied? For this, we first used the homogeneous ICs where the validity condition of the $sQSSA_o$ is not satisfied at any point (Fig 2G). Obviously, the $sQSSA_p$ overestimates both P and $\bar{P}$ of the full model (Fig 2H and 2I). In contrast, the $tQSSA_p$ accurately captures the dynamics of the full model (Fig 2H and 2I).

Now, we heterogenized the ICs while maintaining the spatial average concentrations of Fig 2G (Fig 2J). Specifically, by altering the distribution of S and E, we made the validity condition of the $sQSSA_o$ be satisfied for $x < 15\mu m$, but not for $x > 15\mu m$. With these heterogeneous ICs, unexpectedly, the $sQSSA_p$ accurately captures the dynamics of the full model (Fig 2K and 2L). This is because most of S is localized where the validity condition of the $sQSSA_o$ is satisfied, and thus the majority of P is generated in the valid region (Fig 2J, blue region). As a result, the $sQSSA_p$ can accurately simulate the production rate of P. The $tQSSA_p$ also accurately captures the dynamics of the full model (Fig 2K and 2L).

Taken together, the validity of the $sQSSA_p$ critically depends on the spatial distribution of the ICs. The $sQSSA_p$ can be invalid even when the spatial average concentration satisfies the validity condition of the $sQSSA_o$ ($\bar{E}_T \ll \bar{S}_T + K_M$), and conversely, the $sQSSA_p$ can be valid even when $\bar{E}_T \ll \bar{S}_T + K_M$ is not satisfied. Therefore, using the validity condition of the $sQSSA_o$ based on spatial average concentrations of species is not enough to determine the validity of the $sQSSA_p$. On the other hand, the $tQSSA_p$ is accurate regardless of the spatial distribution of the ICs.

Unlike the $tQSSA_p$, the $sQSSA_p$ may not be applicable in the *in vivo* environment where the enzyme is localized

In the previous section, we demonstrated that the validity of the $sQSSA_p$ cannot be ensured solely by the spatial average concentrations when species are not homogeneously distributed within a domain. This situation is common within cells, as specific enzymes are localized within distinct subcellular organelles such as the nucleus, the ER, lysosomes, and mitochondria (Fig 3A). For instance, in hepatocytes, cytochrome P450 enzymes, which metabolize drugs, are localized in the ER [25].

To mimic *in vivo* environments with the localized enzyme distribution, we utilized the ICs where the enzyme is localized in a narrow region near $x = 15\mu m$ (Fig 3B, dashed line), while the substrate is uniformly distributed throughout the entire cell (Fig 3B, solid line). The ICs do not satisfy the validity condition of the $sQSSA_o$ in a narrow region near $x = 15\mu m$. As a result, the $sQSSA_p$ model overestimates the production of P (Fig 3C and 3D). This is because the majority of the P is produced in the region where the enzyme is localized, and thus $sQSSA_o$ is not valid. However, the $tQSSA_p$ model accurately captures the dynamics of the full model (Fig 3C and 3D). Taken together, it is safer to use the $tQSSA_p$ model than the $sQSSA_p$ model in an *in vivo* environment.

In vitro experiments are usually performed with enzyme and substrate concentrations similar to those in *in vivo* experiments. To mimic this *in vitro* environment, we homogenized the ICs in Fig 3B while maintaining the spatial average concentrations (Fig 3E). With this homogenization, the validity condition of the $sQSSA_o$ ($E_T \ll S_T + K_M$) is satisfied throughout the domain. As a result, not surprisingly, in this case, both the $sQSSA_p$ and $tQSSA_p$ models accurately approximate the dynamics of the full model (Fig 3F and 3G). This indicates that although the $sQSSA_p$ model provides a precise approximation of the full model in *in vitro*, it cannot be directly translated to the *in vivo* environment. This is consistent with previous studies showing that utilizing $sQSSA_o$ to extrapolate *in vitro* drug clearance to *in vivo* drug clearance results in a substantial overestimation of the drug clearance, while the $tQSSA_o$ model provides a reliable estimate for drug clearance [40, 41].

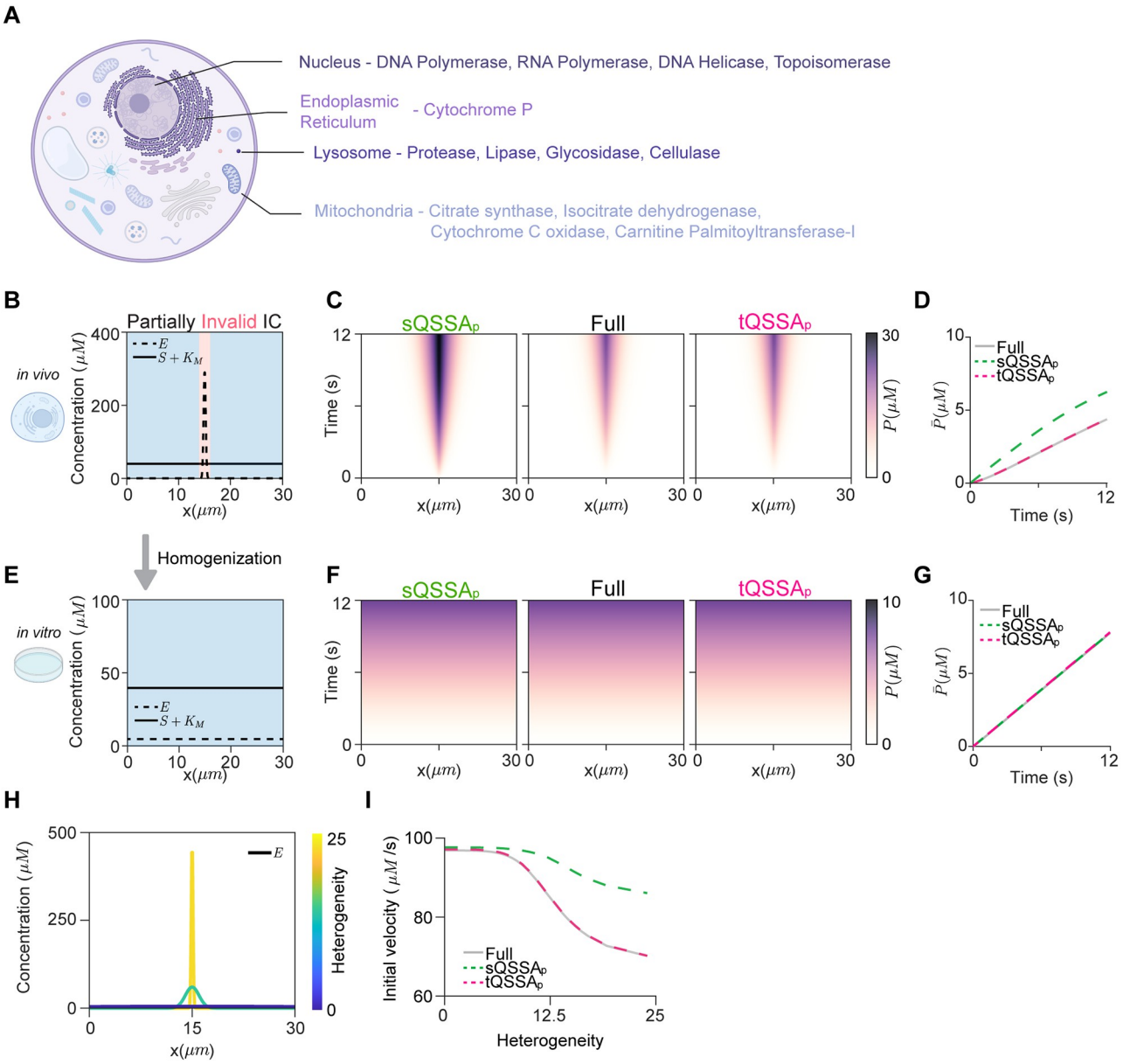

Fig 3. The $sQSSA_p$, but not the $tQSSA_p$, poses a risk when the enzyme is localized within cells, unlike in an *in vitro* experiment. **(A)** Enzymes localized within cellular organelles. **(B)** The heterogeneous ICs where the $sQSSA_o$ are invalid near $x = 15\mu m$ (red region) but valid in the other region (blue region). Here $S_0 \equiv 39\ \mu M$, $E_0(x) = 5 \cdot f(x)\mu M$, where $f(x)$ is the normalized probability density function of the normal distribution with the mean of 15 μm and the standard deviation of 0.2 μm. **(C-D)** Unlike the $sQSSA_p$ model, the $tQSSA_p$ model accurately captures the production of P throughout the domain (C) and its spatial average $\bar{P}$ (D). **(E)** The ICs in (B) were homogenized so that the validity condition of the $sQSSA_o$ is satisfied throughout the domain while maintaining the spatial average concentration. Specifically, $S_0 \equiv 39\ \mu M$ and $E_0 \equiv 5\mu M$ were used. **(F-G)** Both the $sQSSA_p$ and $tQSSA_p$ models are accurate. **(H)** Enzyme distributions with varying heterogeneity were constructed using $E_0(x) = 5 \cdot f(x|\sigma)\ \mu M$, where $f(x|\sigma)$ is the normalized probability density function of the normal distribution with the mean of $15\mu m$ and the standard deviation of σ. As σ decreases, the heterogeneity increases (see Method for details). **(I)** For the enzyme distribution with varying heterogeneity, the $tQSSA_p$ model, but not the $sQSSA_p$ model, accurately captures the initial velocity (I). For all simulations, we used $k_f = 6.7 \cdot 10^5 M^{-1}s^{-1}$, $k_b = 0.53s^{-1}$, $k_{cat} = 0.13s^{-1}$, $K_M = 1\mu M$, and the diffusion coefficients: $D_E = D_C = 0\mu m^2/s$, and $D_P = D_S = 0.2\mu m^2/s$. Some parts of Fig 3 were retrieved from Biorender.

https://doi.org/10.1371/journal.pcbi.1012205.g003

Furthermore, in *in vivo* environments, directly measuring enzyme concentrations throughout cells (e.g., CYP in hepatocytes) is challenging. In the absence of such information, one can investigate how drug clearance changes depending on the heterogeneity of the enzyme distribution in the cell. As the heterogeneity of the initial distribution of E increases (Fig 3H), the initial velocity of production formation considerably decreases (Fig 3I). This is accurately captured by the tQSSA_p model, but not the sQSSA_p model (Fig 3I). This indicates that the sQSSA_p model tends to overestimate drug clearance to a larger extent as the cellular environment becomes more heterogeneous.

Unlike the tQSSA_p, the sQSSA_p can create artificial ultrasensitivity and spatial patterns

So far, we have investigated how the accuracy of QSSAs can vary in a simple enzyme-catalyzed model. Here, we examined biological systems that encompass multiple enzymes, which can exhibit complex behaviors, such as ultrasensitivity, bistability, and oscillation [42]. One prominent example of such reactions is the Goldbeter–Koshland (GK) mechanism (Fig 4A). The GK mechanism describes two interlocked enzyme-catalyzed reactions with a single substrate [11, 43]. Specifically, the substrate (S) is phosphorylated by the kinase (E), and the phosphorylated substrate (S_P) is dephosphorylated by the phosphatase (D). We extended the GK mechanism to the PDE system to represent the spatial distribution of species within the cell in a two-dimensional domain ($\Omega = (0, L) \times (0, L)$) and derived its sQSSA_p and tQSSA_p models (Fig 4A) (see Methods for details).

We explored whether the sQSSA_p and the tQSSA_p models capture the behaviors of the full model across varying concentrations of substrate and enzymes. Specifically, we divided the domain into two regions and gave them two different ICs: one with a high S_T/D_T ratio ($y \geq 15\mu m$), and another with a small S_T/D_T ratio ($y < 15\mu m$) (Fig 4B(i)). As a result, the ICs satisfy the validity condition of the sQSSA_o in $y \geq 15\mu m$ (i.e., $\frac{D_T}{K_{MD}+S_T} \approx 0.02 \ll 1$), but not in $y < 15\mu m$ ($\frac{D_T}{K_{MD}+S_T} \approx 1$).

In $y \geq 15\mu m$, as E_T/D_T increases in a horizontal direction (Fig 4B(ii)), the full model exhibits zero-order ultrasensitivity of phosphorylation at the steady state (Fig 4C(i)). That is, at $E_T/D_T < 1$ ($x < 15\mu m$), the majority of S remains unphosphorylated, and thus the steady-state fraction of total phosphorylated substrate ($\hat{S}_p/S_T$) is close to zero (Fig 4C(i)). On the other hand, when E_T/D_T surpasses 1 at $x = 15\mu m$, the phosphorylation of S becomes suddenly predominant, causing $\hat{S}_p/S_T$ to sharply increase and approach 1 (Fig 4C(i)). This ultrasensitivity is successfully captured by both the tQSSA_p (Fig 4C(ii)) and the sQSSA_p models (Fig 4C(iii)).

In $y < 15\mu m$, the full model does not exhibit ultrasensitivity. That is, $\hat{S}_p/S_T$ gradually increases as E_T/D_T increases and becomes saturated near $x = 15\mu m$, where $E_T/D_T \approx 1$ (Fig 4C (i)). Thus, $\hat{S}_p/S_T$ does not sensitively change around $E_T/D_T \approx 1$. The tQSSA_p accurately captures the smooth changes in phosphorylation of the full model (Fig 4C(ii)). However, the sQSSA_p exhibits an 'artificial' ultrasensitivity (Fig 4C(iii)). That is, using the sQSSA_p to describe the GK mechanism can result in an 'artificial' ultrasensitivity.

Ultrasensitivity is important for pattern formation across various biological and chemical reactions such as cell division [42, 44–46]. We examined how this 'artificial' ultrasensitivity caused by the sQSSA_p affects pattern formation. For this, we used ICs that do not satisfy the validity condition of the sQSSA_o across all regions (i.e., $\frac{D_T}{K_{MD}+S_T} \approx 1$) (Fig 4D(i)). Furthermore, we made ICs of S_T/D_T and E_T/D_T that have horizontal and vertical striped patterns, respectively (Fig 4D(i) and 4D(ii)). Because E_T/D_T changes slightly around one along the x-direction, the full model simulates minimal change of $\hat{S}_p/S_T$ along the x-direction (Fig 4E(i)). On the

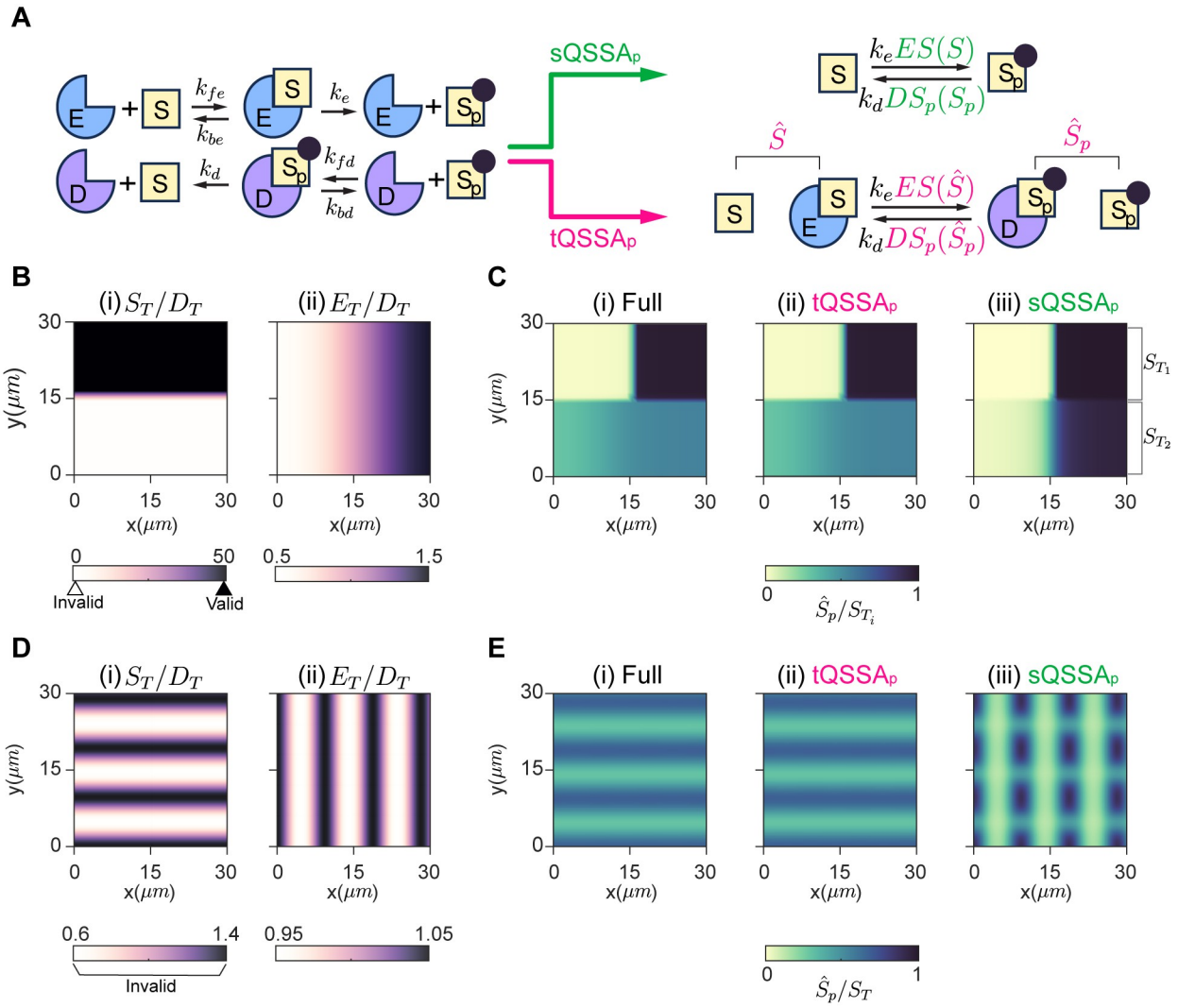

Fig 4. The sQSSA$_p$ generates false patterns due to artificial ultrasensitivity. (A) The model diagram depicting the GK mechanism. The full model (Eq 14) based on mass-action kinetics can be reduced by replacing ES and DS_p with either the sQSSA$_p$ (Eq 15) or the tQSSA$_p$ (Eq 16). **(B)** The heterogeneous ICs where the sQSSA$_o$ is valid in $y > 15\mu m$ (black triangle), but invalid in $y < 15\mu m$ (white triangle). For this, we used $S_0(x, y) = 500\tanh(3.3y - 50) + 520\mu M$, $E_0(x, y) = 10\tanh(0.2x - 3) + 20\mu M$, and $D_0 \equiv 20\mu M$. **(C)** In $y > 15\mu m$, the ultrasensitivity of the full model (i) is accurately captured by both the tQSSA$_p$ (ii) and sQSSA$_p$ models (iii). On the other hand, in $y < 15\mu m$, the sQSSA$_p$ model generates artificial ultrasensitivity (iii) unlike the full (i) and tQSSA$_p$ models (ii). Here, $\hat{S}_p/S_T = S_p/S_T$ for the sQSSA$_p$ model, because DS_p is assumed to be negligible. **(D)** Complex ICs where S_T/D_T exhibits horizontal stripes and E_T/D_T exhibits vertical stripes. These ICs do not satisfy the validity condition of the sQSSA$_o$ throughout the domain. For this, we used $S_0(x, y) = 40\cos(2y/3) + 100\ \mu M$, $E_0(x, y) = 5\cos(2x/3) + 100\mu M$, and $D_0 \equiv 100\ \mu M$. **(E)** The full model (i) and the tQSSA$_p$ model (ii) exhibit horizontally striped patterns. In contrast, the sQSSA$_p$ model (iii) results in a grid pattern due to the artificial ultrasensitivity. (C) and (E) were obtained when $t = 37.5s$. For initial conditions of other species, $S_{p,0} \equiv 0\ \mu M$, $ES_0 \equiv 0\mu M$, and $DS_{p,0} \equiv 0\ \mu M$ were used. In addition, we used $k_{fe} = k_{fd} = 2.22 \cdot 10^6 M^{-1}s^{-1}$, $k_{be} = k_{bd} = 1.84s^{-1}$, $k_e = k_d = 0.38s^{-1}$, $K_{ME} = K_{MD} = 1\mu M$, and $\delta_S = \delta_{S_p} = \delta_{ES} = \delta_{DS_p} = 0.2\mu m^2/s$.

https://doi.org/10.1371/journal.pcbi.1012205.g004

other hand, since S_T/D_T changes considerably along the y-direction, $\hat{S}_p/S_T$ changes considerably along the y-direction. As a result, the full model exhibits a horizontally striped pattern (Fig 4E(i)). This is accurately captured by the tQSSA$_p$ model (Fig 4E(ii)). However, the sQSSA$_p$ model exhibits an artificial grid pattern (Fig 4E(iii)). This artifact arises due to the artificial ultrasensitivity inherent to the sQSSA$_p$. In other words, even slight fluctuations in E_T/D_T

around one cause significant changes in $\hat{S}_p/S_T$ due to this artificial ultrasensitivity (Fig 4C(iii)). Consequently, a vertical striped pattern emerges and combines with the horizontal pattern, resulting in the observed grid-like pattern (Fig 4E(iii)). This indicates that using the MM equation can generate misleading artificial ultrasensitivity and patterns, although it has been frequently utilized to depict pattern formation [47, 48]. Thus, utilizing the tQSSA is a safer option to investigate pattern formation.

Discussion

Although the MM rate law has been the prevalent means for describing enzyme-catalyzed reactions for over a century [5–11], the applicability of the MM rate law remains elusive when species are heterogeneously distributed. However, our study demonstrated that the validity condition of the sQSSA_p (i.e., the MM rate law in a spatiotemporal system) is different from that of the sQSSA_o (Fig 2). Specifically, even if the spatial average concentrations of species satisfy the validity condition of the sQSSA_o, the sQSSA_p model can be inaccurate. And conversely, the sQSSA_p model can be accurate even if the spatial average concentrations do not satisfy the validity condition of the sQSSA_o. Thus, the validity condition based on spatial average concentration does not ensure the accuracy of the sQSSA_p model. Therefore, to assure its accuracy, it is necessary to verify that ICs satisfy the validity condition of the sQSSA_o at each point in the domain. However, this is not feasible because it is challenging to measure concentrations at every point in the cell. Thus, since the tQSSA_p is valid in most cases, our findings suggest that the tQSSA_p offers the best way to reduce and investigate spatiotemporal models.

For systems with fast diffusion, the dynamics of PDE and ODE models are very similar because the concentrations of each species homogenize quickly [26]. In such systems, the validity condition of the sQSSA_p would be similar to that of the sQSSA_o. However, we found that for systems with slow diffusion, the validity of the sQSSA_p becomes different from the sQSSA_o (Figs 2 and 4). This indicates that in models involving slow diffusion, such as 1) measuring dopamine concentration in the brain [49] and 2) detecting current differences with biosensors [50–52], the MM rate law could be inaccurate even when the validity condition of the sQSSA_o is satisfied. Thus, when reducing spatiotemporal models with slow diffusion, it is safer to use the tQSSA_p than the sQSSA_o to avoid potential inaccuracies.

Drugs administered into the body are primarily broken down by CYP enzymes located in liver cells [25]. Drug clearance serves as a key pharmacokinetic parameter for predicting human systemic drug disposition, as cited in over 65,000 papers [40, 42, 53–55]. While the MM rate law has conventionally been used to estimate drug clearance, its validity in drug clearance has only recently been verified [40, 41]. Recent studies suggested that this approach is only valid when the spatial average CYP concentration is significantly smaller than the MM constant of the drug (i.e., $\bar{E}_T/K_M < 0.1$) [40, 41]. Otherwise, the tQSSA model should be used to predict the drug clearance [40, 41]. However, our findings indicate that this criterion for using the MM rate law, based on the spatial average concentration, can be misleading because the liver cell is heterogeneous (Fig 3). Therefore, even when $\bar{E}_T/K_M < 0.1$ is satisfied, utilizing the tQSSA_p may be a safer approach for predicting drug clearance.

In experimental settings including *in vivo* environments, accurately measuring concentrations of substances within cells poses a challenge, which hampers the investigation of how spatial differences affect enzyme-catalyzed reactions. While utilizing various initial conditions can represent different levels of heterogeneity, simulating the full model, encompassing all binding and unbinding interactions, is computationally expensive. Therefore, employing simplified models using sQSSA_p or tQSSA_p is more efficient. However, the sQSSA_p model may not accurately reflect the behavior of the full model in the presence of spatial heterogeneity. For

example, our simulation showed that the $sQSSA_p$ model underestimated the impact of spatial heterogeneity on the initial velocity of enzyme-catalyzed reactions (Fig 3H and 3I). Thus, using the $tQSSA_p$ model, which accurately captures the behavior of the full model regardless of spatial heterogeneity, is a reasonable solution. Indeed, the $tQSSA_p$ model accurately captures the range of the initial velocities of enzyme-catalyzed reactions depending on the spatial heterogeneity of enzyme distributions (Fig 3I).

We have investigated whether QSSAs in the PDE system provide accurate approximations when species are heterogeneously distributed (Figs 2–4). Our work shows that the accuracy of the $tQSSA_p$ model, but not the $sQSSA_p$ model, is not affected by the heterogeneity level. However, to determine whether this result is valid universally, it would be essential to investigate this with a broader range of conditions. Furthermore, our findings are based on numerical simulations rather than theoretical derivations. Notably, recent theoretical studies have identified a small region where the $tQSSA_o$ becomes inaccurate, although the $tQSSA_o$ has been believed to be generally accurate [33, 56]. Therefore, the theoretical investigation of the validity of the $tQSSA_p$ should be a crucial focus for future research. Furthermore, a recent study proposed a more accurate model than the MM rate law by using the effective time-delay scheme [57]. Investigating this new scheme in heterogeneous environments would be also interesting in future work.

Even when the $tQSSA_p$ accurately approximates the original PDE systems, the $tQSSA_p$ may not be accurate in a stochastic context. Using the $tQSSA_o$ for stochastic simulations is usually accurate [11, 58–64] and thus has been widely used [65–68]. However, a recent study has shown that using the $tQSSA_o$ for stochastic simulations can be inaccurate even though it is accurate in a deterministic simulation in which the molar ratio of E and S is close to 1:1 and their binding is tight [69]. This implies that the validity condition of the $tQSSA_o$ in stochastic systems is different from that in deterministic systems. Therefore, it would be interesting in future work to investigate the validity of the $tQSSA_p$ in deterministic and stochastic contexts.

Materials and methods

Numerical simulation for a simple enzyme-catalyzed reaction model (1-D model)

In Figs 2 and 3, to simulate the enzyme-catalyzed reaction, we numerically solved PDE systems (Eqs 9, 11 and 13) in a one-dimensional space $\Omega = (0, L)$. Let $x_j = j\Delta x = jL/(N_x - 1)$ be the N_x-equispaced grids in Ω, which are referred to as the Fourier collocation points, to implement the cosine-based spectral method. The time step Δt was defined as $\Delta t = T/N_t$, where T is the final time and N_t is the total number of time steps. We denote the numerical approximation of $S(n\Delta t, x)$, $E(n\Delta t, x)$, $C(n\Delta t, x)$, $P(n\Delta t, x)$ by S^n, E^n, C^n, P^n, respectively.

To facilitate simulation, we split PDE systems into diffusion and reaction parts using the operator splitting method [70]. That is, for each time step of the simulation, the diffusion and reaction were calculated separately. We first calculated the diffusion parts in Eqs 9, 11, and 13 as follows:

$$\frac{S^* - S^n}{\Delta t} = D_S \Delta S^*,$$
$$\frac{E^* - E^n}{\Delta t} = D_E \Delta E^*,$$
$$\frac{C^* - C^n}{\Delta t} = D_C \Delta C^*,$$
$$\frac{P^* - P^n}{\Delta t} = D_P \Delta P^*.$$

After obtaining S^*, E^*, C^*, and P^* by calculating the diffusion part, the reaction parts were calculated to obtain S^{n+1}, E^{n+1}, C^{n+1}, and P^{n+1}. Specifically, for the full model (Eq 9), the following reaction equations were used.

$$\begin{aligned}
\frac{S^{n+1}-S^*}{\Delta t} &= -k_f E^* S^* + k_b C^*,\\
\frac{E^{n+1}-E^*}{\Delta t} &= -k_f E^* S^* + k_b C^* + k_{cat} C^*,\\
\frac{C^{n+1}-C^*}{\Delta t} &= k_f E^* S^* - k_b C^* - k_{cat} C^*,\\
\frac{P^{n+1}-P^*}{\Delta t} &= k_{cat} C^*.
\end{aligned}$$

For the sQSSA$_p$ model (Eq 11), we defined $E_T^* = E^* + C^*$ and $C^*(S^*) = \frac{E_T^* S^*}{S^* + K_M}$ to calculate the reaction parts. Then, we obtained S^{n+1} and P^{n+1} as follows:

$$\begin{aligned}
\frac{S^{n+1}-S^*}{\Delta t} &= -k_{cat} C^*(S^*),\\
\frac{P^{n+1}-P^*}{\Delta t} &= k_{cat} C^*(S^*).
\end{aligned}$$

Furthermore, using S^{n+1} and P^{n+1}, we obtained $C^{n+1} = \frac{E_T^* S^{n+1}}{(S^{n+1}+K_M)}$, and $E^{n+1} = E_T^* - C^{n+1}$.

For the tQSSA$_p$ model (Eq 13), we defined $E_T^* = E^* + C^*$, $\hat{S}^* = S^* + C^*$ and $C^*(\hat{S}^*) = \frac{1}{2}\left[E_T^* + \hat{S}^* + K_M - \sqrt{(E_T^* + \hat{S}^* + K_M)^2 - 4E_T^* \hat{S}^*}\right]$ to calculate the reaction part. Then the following reaction equations were used to obtain $\hat{S}^{n+1}$ and P^{n+1}.

$$\begin{aligned}
\frac{\hat{S}^{n+1}-\hat{S}^*}{\Delta t} &= -k_{cat} C^*(\hat{S}^*),\\
\frac{P^{n+1}-P^*}{\Delta t} &= k_{cat} C^*(\hat{S}^*).
\end{aligned}$$

Then, using $\hat{S}^{n+1}$ and P^{n+1}, we obtained $C^{n+1} = \frac{1}{2}\left[E_T^* + \hat{S}^{n+1} + K_M - \sqrt{(E_T^* + \hat{S}^{n+1} + K_M)^2 - 4E_T^* \hat{S}^{n+1}}\right]$, $E^{n+1} = E_T^* - C^{n+1}$, and $S^{n+1} = \hat{S}^{n+1} - C^{n+1}$ for the next time step.

For Fig 2, we simulated with $k_f = 3.4\mu M^{-1}s^{-1}$, $k_b = 60s^{-1}$, and $k_{cat} = 3.2s^{-1}$; thus, the MM constant $K_M = 18.5\mu M$. Furthermore, we used $L = 30\mu m$, $T = 1.25s$, $N_x = 100$, $N_t = 2730$, resulting in $\Delta x = 0.3\mu m$ and $\Delta t = 4.6 \cdot 10^{-4}s$. Diffusion coefficients of $D_E = D_S = D_C = D_P = 0.2\mu m^2/s$ were used. For Fig 3, we simulated with $k_f = 0.67\mu M^{-1}s^{-1}$, $k_b = 0.53s^{-1}$, $k_{cat} = 0.13s^{-1}$, $K_M = 1\mu M$. Moreover, we used the parameter $L = 30\mu m$, $T = 12s$, $N_x = 300$, $N_t = 11921$, resulting in $\Delta x = 0.1\mu m$, $\Delta t = 0.001s$, and assumed that the substrate spread quickly $D_P = D_S = 0.2\mu m^2/s$, $D_E = D_C = 0\mu m^2/s$.

For Fig 3H and 3I, we utilized various spatial distributions of enzymes. Specifically, the enzyme concentration was described by the normalized probability density function of the normal distribution with the mean of $15\mu m$ and the standard deviation of σ: $E_0(x) = 5f(x|\sigma)$ (μM), where $f(x|\sigma) = \frac{f_0(x|\sigma)}{\int_0^{30} f_0(x|\sigma)dx}$ and $f_0(x|\sigma) = \frac{1}{\sigma\sqrt{2\pi}}\exp\left(-\frac{(x-15)^2}{2\sigma^2}\right)$. Then, the heterogeneity of

the E_0 was defined as follows:

$$\text{hetrogeneity} \quad = 10\log\left(\frac{\sigma_{\max}}{\sigma}\right),$$

where σ is the standard deviation of the normal distribution, and we set $\sigma_{\max} = 25\mu m$ since E becomes almost constant across the space when $\sigma \geq 25\mu m$.

Additionally, we measured the initial velocity of the enzyme-catalyzed reaction as the average reaction velocity over the first 12 seconds from the initial state, by using: $\frac{\bar{P}(t=12s)}{12s}$.

PDE model describing the GK mechanism

In Fig 4, we extended the GK mechanism [11, 43], which consists of two interconnected, single-substrate, enzyme-catalyzed reactions, to the PDE model as follows:

$$\begin{aligned}
\frac{\partial S}{\partial t} &= \delta_S \Delta S - k_{fe} S \cdot E + k_{be} ES + k_d DS_p, \\
\frac{\partial S_p}{\partial t} &= \delta_{S_p} \Delta S_p - k_{fd} S_p \cdot D + k_{bd} DS_p + k_e ES, \\
\frac{\partial E}{\partial t} &= -k_{fe} S \cdot E + k_{be} ES + k_e ES, \\
\frac{\partial D}{\partial t} &= -k_{fd} S_p \cdot D + k_{bd} DS_p + k_d DS_p, \\
\frac{\partial ES}{\partial t} &= \delta_{ES} \Delta ES + k_{fe} S \cdot E - k_{be} ES - k_e ES, \\
\frac{\partial DS_p}{\partial t} &= \delta_{DS_p} \Delta DS_p + k_{fd} S_p \cdot D - k_{bd} DS_p - k_d DS_p,
\end{aligned} \tag{14}$$

where δ_S, δ_{S_p}, δ_{ES}, and δ_{DS_p} denote the diffusion coefficients of S, S_p, ES, and DS_p, respectively. We assumed that the enzymes (D and E) do not diffuse. Furthermore, similar to the simple enzyme-catalyzed reaction (Eq 9), zero-Neumann boundary conditions and ICs were used with $S(0, x, y) = S_0(x, y)$, $S_p(0, x, y) = S_{p,0}(x, y)$, $E(0, x, y) = E_0(x, y)$, $D(0, x, y) = D_0(x, y)$, $ES(0, x, y) = ES_0(x, y)$, and $DS_p(0, x, y) = DS_{p,0}(x, y)$.

In this model, $S_T = S + S_p + ES + DS_p$, $E_T = E + ES$, and $D_T = D + DS_p$ are concentrations of total substrate and product, total kinase, and total phosphatase, respectively. This full model (Eq 14) can also be reduced by applying the sQSSA_p, as done in the simple enzyme model (Fig 4A). In particular, ES and DS_p are assumed to reach each QSS, resulting in QSSA of $ES(S) = \frac{E_T S}{S + K_{ME}}$, and $DS_p(S_p) = \frac{D_T S_p}{S_p + K_{MD}}$, where $K_{ME} = (k_{be} + k_e)/k_{fe}$, $K_{MD} = (k_{bd} + k_d)/k_{fd}$. This

results in the rates of phosphorylation and dephosphorylation in terms of E_T, D_T, S, and S_p:

$$\begin{aligned}\frac{\partial S}{\partial t} &= \delta_S \Delta S - k_e ES(S) + k_d DS_p(S_p),\\ \frac{\partial S_p}{\partial t} &= \delta_{S_p} \Delta S_p + k_e ES(S) - k_d DS_p(S_p),\\ \frac{\partial E_T}{\partial t} &= \delta_{ES} \Delta ES(S),\\ \frac{\partial D_T}{\partial t} &= \delta_{DS_p} \Delta DS_p(S_p).\end{aligned} \tag{15}$$

Alternatively, we introduce $\hat{S} = S + ES$ and $\hat{S}_p = S_p + DS_p$ and apply the tQSSA$_p$ by substituting ES and DS_p with $ES(\hat{S}) = \frac{1}{2}\left[E_T + \hat{S} + K_{ME} - \sqrt{(E_T + \hat{S} + K_{ME})^2 - 4E_T\hat{S}}\right]$ and $DS_p(\hat{S}_p) = \frac{1}{2}\left[D_T + \hat{S}_p + K_{MD} - \sqrt{(D_T + \hat{S}_p + K_{MD})^2 - 4D_T\hat{S}_p}\right]$, respectively. Then we obtain the following reduced model of the GK mechanism:

$$\begin{aligned}\frac{\partial \hat{S}}{\partial t} &= \delta_S \Delta(\hat{S} - ES(\hat{S})) + \delta_{ES} \Delta(ES(\hat{S})) - k_e ES(\hat{S}) + k_d DS_p(\hat{S}_p)\\ \frac{\partial \hat{S}_p}{\partial t} &= \delta_{S_p} \Delta(\hat{S}_p - DS_p(\hat{S}_p)) + \delta_{DS_p} \Delta(DS_p(\hat{S}_p)) + k_e ES(\hat{S}) - k_d DS_p(\hat{S}_p),\\ \frac{\partial E_T}{\partial t} &= \delta_{ES} \Delta ES(\hat{S}),\\ \frac{\partial D_T}{\partial t} &= \delta_{DS_p} \Delta DS_p(\hat{S}_p).\end{aligned} \tag{16}$$

Numerical simulation for the model describing the GK mechanism (2-D model)

In Fig 4, we simulated a two-dimensional multi-enzyme model. Similar to the 1-D model, we discretized a spatial variable in a two-dimensional spatial domain $\Omega = (0, L) \times (0, L)$ by using the cosine-based spectral method with a uniform mesh size $\Delta x = L/(N_x - 1)$, $\Delta y = L/(N_y - 1)$, where $N_x, N_y \in \mathbb{N}$. Let the numerical approximation of $S^n = S(n\Delta t, x, y)$, ${S_p}^n = S_p(n\Delta t, x, y)$, $E^n = E(n\Delta t, x, y)$, $D^n = D(n\Delta t, x, y)$, $ES^n = ES(n\Delta t, x, y)$, and ${DS_p}^n = DS_p(n\Delta t, x, y)$.

Similar to Figs 2 and 3, we utilized the operator splitting method and spectral method. Therefore, the diffusion and reaction were still calculated separately for each time step. We

first calculated the diffusion parts in Eqs 14–16 as follows:

$$\begin{aligned}\frac{S^* - S^n}{\Delta t} &= \delta_S \Delta S^*,\\ \frac{S_p^* - S_p^n}{\Delta t} &= \delta_{S_p} \Delta S_p^*,\\ \frac{ES^* - ES^n}{\Delta t} &= \delta_{ES} \Delta ES^*,\\ \frac{DS_p^* - DS_p^n}{\Delta t} &= \delta_{DS_p} \Delta DS_p^*.\end{aligned}$$

After obtaining S^*, S_p^*, ES^*, and DS_p^* by calculating the diffusion part, the reaction parts were calculated to obtain S^{n+1}, S_p^{n+1}, E^{n+1}, D^{n+1}, ES^{n+1}, and DS_p^{n+1}. Specifically, for the full model (Eq 14), the following reaction equations were used.

$$\begin{aligned}\frac{S^{n+1} - S^*}{\Delta t} &= -k_{fe} S^* E^n + k_{be} ES^* + k_d DS_p{}^*,\\ \frac{S_p^{n+1} - S_p^*}{\Delta t} &= -k_{fd} S_p^* D^n + k_{bd} DS_p^* + k_e ES^*,\\ \frac{E^{n+1} - E^n}{\Delta t} &= -k_{fe} S^* E^n + (k_{be} + k_e) ES^*,\\ \frac{D^{n+1} - D^n}{\Delta t} &= -k_{fd} S_p^* D^n + (k_{bd} + k_d) DS_p^*,\\ \frac{ES^{n+1} - ES^*}{\Delta t} &= k_{fe} E^n S^* - k_{be} ES^* - k_e ES^*,\\ \frac{DS_p^{n+1} - DS_p^*}{\Delta t} &= k_{fd} D^n S_p^* - k_{bd} DS_p^* - k_d DS_p^*.\end{aligned}$$

In the sQSSA_p model (Eq 15), we defined $E_T^* = E^n + ES^*$, $D_T^* = D^n + DS_p^*$, $ES^*(S^*) = \frac{E_T^* S^*}{S^* + K_{ME}}$, and $DS_p^*(S_p^*) = \frac{D_T^* S_p^*}{S_p^* + K_{MD}}$. Then, we obtained S^{n+1}, S_p^{n+1} as follows:

$$\begin{aligned}\frac{S^{n+1} - S^*}{\Delta t} &= -k_e ES^*(S^*) + k_d DS_p^*(S_p^*),\\ \frac{S_p^{n+1} - S_p^*}{\Delta t} &= k_e ES^*(S^*) - k_d DS_p^*(S_p^*).\end{aligned}$$

For the tQSSA_p model (Eq 16), we defined $E_T^* = E^n + ES^*$, $D_T^* = D^n + DS_p^*$, $\hat{S}^* = S^* + ES^*$, $\hat{S}_p^* = S_p^* + DS_p^*$, $ES^*(\hat{S}^*) = \frac{1}{2}\left[E_T^* + \hat{S}^* + K_{ME} - \sqrt{(E_T^* + \hat{S}^* + K_{ME})^2 - 4E_T^* \hat{S}^*}\right]$, and $DS_p^*(\hat{S}_p^*) = \frac{1}{2}\left[D_T^* + \hat{S}_p^* + K_{MD} - \sqrt{(D_T^* + \hat{S}_p^* + K_{MD})^2 - 4D_T^* \hat{S}_p^*}\right]$. Then, we obtained $\hat{S}^{n+1}$, $\hat{S}_p^{n+1}$ as follows:

$$\frac{\hat{S}^{n+1} - \hat{S}^*}{\Delta t} = -k_e ES^*(\hat{S}^*) + k_d DS_p^*(\hat{S}_p^*), \tag{17}$$

$$\frac{\hat{S}_p^{n+1} - \hat{S}_p^*}{\Delta t} = k_e ES^*(\hat{S}^*) - k_d DS_p^*(\hat{S}_p^*). \tag{18}$$

For simulations, we used $k_{fe} = k_{fd} = 2.22\mu M^{-1}\, s^{-1}$, $k_{be} = k_{bd} = 1.84s^{-1}$, $k_d = k_e = 0.38s^{-1}$, $K_{ME} = K_{MD} = 1\mu M$, and $\delta_S = \delta_{S_p} = \delta_{ES} = \delta_{DS_p} = 0.2\mu m^2/s$. For discretization in space and time for Figs 4B and 4C, we used $L = 30\mu m$, $T = 1{,}100s$, $N_x = N_y = 30$, $N_t = 100{,}000$, resulting in $\Delta x = \Delta y = 1\mu m$, $\Delta t = 0.011s$ and the diffusion coefficients $\delta_S = \delta_{S_p} = \delta_{ES} = \delta_{DS_p} = 0.2\mu m^2/s$. For Fig 4D and 4E, we used $L = 30\mu m$, $T = 8.33s$, $N_x = N_y = 50$, $N_t = 200{,}000$, resulting in $\Delta x = \Delta y = 0.6\mu m$, $\Delta t = 0.00004s$.

The computational codes for implementing all of the models used in this study can be found at https://github.com/Mathbiomed/PDE_QSSA.

Supporting information

S1 Fig. The $sQSSA_p$ model becomes inaccurate in heterogeneous environments, as long as the diffusion is slower than the slow reactions. The spatial average concentration of the product ($\bar{P}$) of the full model and that obtained from the $sQSSA_p$ and $tQSSA_p$ models were compared under varying diffusion coefficients (D_*). Specifically, D_* was varied across a wide range, from $2 \cdot 10^{-5}\mu m^2/s$ to $2 \cdot 10^{4}\mu m^2/s$, leading to a change in diffusion time scale (L^2/D_*) from $4.5 \cdot 10^{7}s$ to $4.5 \cdot 10^{-2}s$. When the L^2/D_* is $\sim$100-fold larger than the time scale of the slow reaction ($k_{cat}^{-1} = 0.31s$), the $sQSSA_p$ model overestimates $\bar{P}$, compared to the full model and the $tQSSA_p$ model. When the L^2/D_* is similar to or shorter than the time scale of the slow reaction, the $sQSSA_p$ model also provides accurate results compared to the full model and the $tQSSA_p$ model because the PDE behaves similarly to the ODE due to homogenization via fast diffusion.
(TIF)

Author Contributions

Conceptualization: Seunggyu Lee, Jae Kyoung Kim.

Data curation: Seolah Shin, Seok Joo Chae.

Formal analysis: Seolah Shin, Seok Joo Chae, Seunggyu Lee, Jae Kyoung Kim.

Funding acquisition: Seunggyu Lee, Jae Kyoung Kim.

Investigation: Seolah Shin, Seok Joo Chae, Seunggyu Lee, Jae Kyoung Kim.

Methodology: Seolah Shin, Seok Joo Chae, Seunggyu Lee, Jae Kyoung Kim.

Project administration: Seunggyu Lee, Jae Kyoung Kim.

Resources: Seunggyu Lee, Jae Kyoung Kim.

Software: Seolah Shin, Seok Joo Chae.

Supervision: Seunggyu Lee, Jae Kyoung Kim.

Validation: Seolah Shin, Seok Joo Chae, Seunggyu Lee, Jae Kyoung Kim.

Visualization: Seolah Shin, Seok Joo Chae, Seunggyu Lee, Jae Kyoung Kim.

Writing – original draft: Seolah Shin, Seok Joo Chae, Seunggyu Lee, Jae Kyoung Kim.

Writing – review & editing: Seolah Shin, Seok Joo Chae, Seunggyu Lee, Jae Kyoung Kim.

References

1. Griffiths AJ. Modern genetic analysis: integrating genes and genomes. vol. 1. Macmillan; 2002.

2. Kirk O, Borchert TV, Fuglsang CC. Industrial enzyme applications. Curr Opin Biotechnol. 2002; 13 (4):345–351. https://doi.org/10.1016/S0958-1669(02)00328-2 PMID: 12323357
3. Heinen L, Heuser T, Steinschulte A, Walther A. Antagonistic Enzymes in a Biocatalytic pH Feedback System Program Autonomous DNA Hydrogel Life Cycles. Nano Lett. 2017; 17(8):4989–4995. https://doi.org/10.1021/acs.nanolett.7b02165 PMID: 28656771
4. Cooper GM, Adams KW. The cell: a molecular approach. Oxford University Press; 2023.
5. Henri V. Lois générales de l'action des diastases. Librairie Scientifique A. Hermann; 1903.
6. Michaelis L, Menten ML. Die kinetik der invertinwirkung. Biochem Z. 1913; 49(333-369):352.
7. Briggs GE, Haldane JBS. A Note on the Kinetics of Enzyme Action. Biochem J. 1925; 19(2):338–339. https://doi.org/10.1042/bj0190338 PMID: 16743508
8. Biaglow A, Erickson K, McMurran S. Enzyme Kinetics and the Michaelis-Menten Equation. PRIMUS. 2010; 20(2):148–168. https://doi.org/10.1080/10511970903486491
9. Johnson KA, Goody RS. The Original Michaelis Constant: Translation of the 1913 Michaelis–Menten Paper. Biochemistry. 2011; 50(39):8264–8269. https://doi.org/10.1021/bi201284u PMID: 21888353
10. Cornish-Bowden A. One hundred years of Michaelis–Menten kinetics. Perspectives in Science. 2015; 4:3–9. https://doi.org/10.1016/j.pisc.2014.12.002
11. Kim JK, Tyson JJ. Misuse of the Michaelis–Menten rate law for protein interaction networks and its remedy. PLoS Comput Biol. 2020; 16(10):1–21. https://doi.org/10.1371/journal.pcbi.1008258 PMID: 33090989
12. Segel LA, Slemrod M. The Quasi-Steady-State Assumption: A Case Study in Perturbation. SIAM Rev. 1989; 31(3):446–477. https://doi.org/10.1137/1031091
13. Schnell S, Maini P. A Century of Enzyme Kinetics: Reliability of the KM and vmax Estimates. Comments Theor. Biol. 2003; 8.
14. Tzafriri AR. Michaelis–Menten kinetics at high enzyme concentrations. Bull Math Biol. 2003; 65 (6):1111–1129. https://doi.org/10.1016/S0092-8240(03)00059-4 PMID: 14607291
15. Bolouri H, Davidson EH. Modeling transcriptional regulatory networks. BioEssays. 2002; 24(12):1118–1129. https://doi.org/10.1002/bies.10189 PMID: 12447977
16. Rué P, Garcia-Ojalvo J. Modeling Gene Expression in Time and Space. Annu Rev Biophys. 2013; 42 (1):605–627. https://doi.org/10.1146/annurev-biophys-083012-130335 PMID: 23527779
17. Attie AD, Raines RT. Analysis of receptor-ligand interactions. J Chem Educ. 1995; 72(2):119. https://doi.org/10.1021/ed072p119 PMID: 28736457
18. Pollard TD. A Guide to Simple and Informative Binding Assays. Mol Biol Cell. 2010; 21(23):4061–4067. https://doi.org/10.1091/mbc.E10-08-0683 PMID: 21115850
19. Ciliberto A, Capuani F, Tyson JJ. Modeling Networks of Coupled Enzymatic Reactions Using the Total Quasi-Steady State Approximation. PLoS Comput Biol. 2007; 3(3):1–10. https://doi.org/10.1371/journal.pcbi.0030045 PMID: 17367203
20. Cha S. Kinetic Behavior at High Enzyme Concentrations: Magnitude of Errors of Michaelis-Menten and other Approximations. J Biol Chem. 1970; 245(18):4814–4818. https://doi.org/10.1016/S0021-9258(18)62865-0 PMID: 5456154
21. Borghans JAM, de Boer RJ, Segel LA. Extending the quasi-steady state approximation by changing variables. Bull Math Biol. 1996; 58(1):43–63. https://doi.org/10.1007/BF02458281 PMID: 8819753
22. Bersani AM, Bersani E, Dell'Acqua G, Pedersen MG. New trends and perspectives in nonlinear intracellular dynamics: one century from Michaelis–Menten paper. Contin Mech Thermodyn. 2015; 27(4):659–684. https://doi.org/10.1007/s00161-014-0367-4
23. Choi B, Rempala GA, Kim JK. Beyond the Michaelis-Menten equation: Accurate and efficient estimation of enzyme kinetic parameters. Sci Rep. 2017; 7(1):17018. https://doi.org/10.1038/s41598-017-17072-z PMID: 29208922
24. Chen LY, Zhang Y, Zhang Q, Li H, Luo Z, Fang H, et al. Mitochondrial Localization of Telomeric Protein TIN2 Links Telomere Regulation to Metabolic Control. Mol Cell. 2012; 47(6):839–850. https://doi.org/10.1016/j.molcel.2012.07.002 PMID: 22885005
25. Kwon D, Kim SM, Correia MA. Cytochrome P450 endoplasmic reticulum-associated degradation (ERAD): therapeutic and pathophysiological implications. Acta Pharm Sin B. 2020; 10(1):42–60. https://doi.org/10.1016/j.apsb.2019.11.002 PMID: 31993306
26. Kalachev LV, Kaper HG, Kaper TJ, Popovic N, Zagaris A. Reduction for Michaelis-Menten-Henri kinetics in the presence of diffusion. In: asdf, editors. 2006 International Conference in honor of Jacqueline Fleckinger; Electron J Differ Equ. 2007;16:155–184.
27. Frank M, Lax C, Walcher S, Wittich O. Quasi-steady state reduction for the Michaelis–Menten reaction–diffusion system. J Math Chem. 2018; 56(6):1759–1781. https://doi.org/10.1007/s10910-018-0891-8

28. Bothe D, Pierre M. Quasi-steady-state approximation for a reaction–diffusion system with fast intermediate. J Math Anal Appl. 2010; 368(1):120–132. https://doi.org/10.1016/j.jmaa.2010.02.044

29. Eaton SL, Roche SL, Llavero Hurtado M, Oldknow KJ, Farquharson C, Gillingwater TH, et al. Total Protein Analysis as a Reliable Loading Control for Quantitative Fluorescent Western Blotting. PLoS One. 2013; 8(8):1–9. https://doi.org/10.1371/journal.pone.0072457 PMID: 24023619

30. Noble JE. Chapter Two—Quantification of Protein Concentration Using UV Absorbance and Coomassie Dyes. In: Lorsch J, editor. Laboratory Methods in Enzymology: Protein Part A. vol. 536 of Methods in Enzymology. Academic Press; 2014. p. 17–26.

31. Buss H, Chan TP, Sluis KB, Domigan NM, Winterbourn CC. Protein Carbonyl Measurement by a Sensitive ELISA Method. Free Radic Biol Med. 1997; 23(3):361–366. https://doi.org/10.1016/S0891-5849(97)00104-4 PMID: 9214571

32. Bennett MR, Volfson D, Tsimring L, Hasty J. Transient Dynamics of Genetic Regulatory Networks. Biophys J. 2007; 92(10):3501–3512. https://doi.org/10.1529/biophysj.106.095638 PMID: 17350994

33. Eilertsen J, Schnell S. The quasi-steady-state approximations revisited: Timescales, small parameters, singularities, and normal forms in enzyme kinetics. Math Biosci. 2020; 325:108339. https://doi.org/10.1016/j.mbs.2020.108339 PMID: 32184091

34. Kühn T, Ihalainen TO, Hyväluoma J, Dross N, Willman SF, Langowski J, et al. Protein Diffusion in Mammalian Cell Cytoplasm. PLoS One. 2011; 6(8):1–12. https://doi.org/10.1371/journal.pone.0022962 PMID: 21886771

35. Koch AA, Bagnall JS, Smyllie NJ, Begley N, Adamson AD, Fribourgh JL, et al. Quantification of protein abundance and interaction defines a mechanism for operation of the circadian clock. eLife. 2022; 11:e73976. https://doi.org/10.7554/eLife.73976 PMID: 35285799

36. Northrup SH, Erickson HP. Kinetics of protein-protein association explained by Brownian dynamics computer simulation. Proc Natl Acad Sci U S A. 1992; 89(8):3338–3342. https://doi.org/10.1073/pnas.89.8.3338 PMID: 1565624

37. Yao X, Heidebrecht BL, Chen J, Tyson JJ. Mathematical analysis of robustness of oscillations in models of the mammalian circadian clock. PLoS Comput Biol. 2022; 18(3):e1008340. https://doi.org/10.1371/journal.pcbi.1008340 PMID: 35302984

38. Bar-Even A, Noor E, Savir Y, Liebermeister W, Davidi D, Tawfik DS, et al. The moderately efficient enzyme: evolutionary and physicochemical trends shaping enzyme parameters. Biochem. 2011; 50(21):4402–4410. https://doi.org/10.1021/bi2002289 PMID: 21506553

39. Marguerat S, Bähler J. Coordinating genome expression with cell size. Trends Genet. 2012; 28(11):560–565. https://doi.org/10.1016/j.tig.2012.07.003 PMID: 22863032

40. Back HM, Yun HY, Kim SK, Kim JK. Beyond the Michaelis-Menten: Accurate Prediction of In Vivo Hepatic Clearance for Drugs With Low KM. Clin Transl Sci. 2020; 13(6):1199–1207. https://doi.org/10.1111/cts.12804 PMID: 32324332

41. Vu NAT, Song YM, Tran QT, Yun Hy, Kim SK, Chae Jw, et al. Beyond the Michaelis–Menten: Accurate Prediction of Drug Interactions Through Cytochrome P450 3A4 Induction. Clin Pharmacol Ther. 2023; 113(5):1048–1057. https://doi.org/10.1002/cpt.2824 PMID: 36519932

42. Zhang Q, Bhattacharya S, Andersen ME. Ultrasensitive response motifs: basic amplifiers in molecular signalling networks. Open Bio. 2013; 3(4):130031. https://doi.org/10.1098/rsob.130031 PMID: 23615029

43. Goldbeter A, Koshland DE. An amplified sensitivity arising from covalent modification in biological systems. Proc Natl Acad Sci U S A. 1981; 78(11):6840–6844. https://doi.org/10.1073/pnas.78.11.6840 PMID: 6947258

44. Kholodenko BN. Cell-signalling dynamics in time and space. Nat Rev Mol Cell Biol. 2006; 7(3):165–176. https://doi.org/10.1038/nrm1838 PMID: 16482094

45. Kretschmer S, Schwille P. Pattern formation on membranes and its role in bacterial cell division. Curr Opin Cell Biol. 2016; 38:52–59. https://doi.org/10.1016/j.ceb.2016.02.005 PMID: 26915065

46. Li C, Zhang L, Nie Q. Landscape reveals critical network structures for sharpening gene expression boundaries. BMC Systems Biology. 2018; 12(1):67. https://doi.org/10.1186/s12918-018-0595-5 PMID: 29898720

47. Sugai SS, Ode KL, Ueda HR. A Design Principle for an Autonomous Post-translational Pattern Formation. Cell Rep. 2017; 19(4):863–874. https://doi.org/10.1016/j.celrep.2017.03.081 PMID: 28445735

48. Liu B, Wu R, Chen L. Patterns induced by super cross-diffusion in a predator-prey system with Michaelis–Menten type harvesting. Math Biosci. 2018; 298:71–79. https://doi.org/10.1016/j.mbs.2018.02.002 PMID: 29471009

49. Nicholson C. Interaction between diffusion and Michaelis-Menten uptake of dopamine after iontophoresis in striatum. Biophys J. 1995; 68(5):1699–1715. https://doi.org/10.1016/S0006-3495(95)80348-6 PMID: 7612814

50. Lyons M, Bannon T, Hinds G, Rebouillat S. Reaction/diffusion with Michaelis-Menten kinetics in electroactive polymer filmsPart 2.‡ The transient amperometric response. Anal. 1998; 123:1947–1959. https://doi.org/10.1039/a803274b

51. Kirthiga OM, Rajendran L. Approximate analytical solution for non-linear reaction diffusion equations in a mono-enzymatic biosensor involving Michaelis–Menten kinetics. J Electroanal Chem. 2015; 751:119–127. https://doi.org/10.1016/j.jelechem.2015.05.036

52. Swaminathan R, Narayanan KL, Mohan V, Saranya K, Rajendran L. Reaction/Diffusion Equation with Michaelis-Menten Kinetics in Microdisk Biosensor: Homotopy Perturbation Method Approach. Int J Electrochem Sci. 2019; 14(4):3777–3791. https://doi.org/10.20964/2019.04.13

53. Mishra H, Polak S, Jamei M, Rostami-Hodjegan A. Interaction between domperidone and ketoconazole: toward prediction of consequent QTc prolongation using purely in vitro information. CPT Pharmacometrics Syst Pharmacol. 2014; 3(8):1–11. https://doi.org/10.1038/psp.2014.26 PMID: 25116274

54. Benet L, Liu S, Wolfe A. The Universally Unrecognized Assumption in Predicting Drug Clearance and Organ Extraction Ratio. Clin Pharmacol Ther. 2018; 103(3):521–525. https://doi.org/10.1002/cpt.802 PMID: 28762489

55. Horde GW, Gupta V. Drug clearance. StatPearls Publishing; 2020.

56. Eilertsen J, Schnell S, Walcher S. The unreasonable effectiveness of the total quasi-steady state approximation, and its limitations. bioRxiv. 2023; p. 2023–09.

57. Lim R, Martin TLP, Chae J, Kim WJ, Ghim CM, Kim PJ. Generalized Michaelis–Menten rate law with time-varying molecular concentrations. PLoS Comp Biol. 2023; 19(12):1–18. https://doi.org/10.1371/journal.pcbi.1011711 PMID: 38079453

58. Barik D, Paul MR, Baumann WT, Cao Y, Tyson JJ. Stochastic Simulation of Enzyme-Catalyzed Reactions with Disparate Timescales. Biophys J. 2008; 95(8):3563–3574. https://doi.org/10.1529/biophysj.108.129155 PMID: 18621809

59. Gómez-Uribe CA, Verghese GC, Tzafriri AR. Enhanced identification and exploitation of time scales for model reduction in stochastic chemical kinetics. J Chem Phys. 2008; 129(24):244112. https://doi.org/10.1063/1.3050350 PMID: 19123500

60. MacNamara S, Bersani AM, Burrage K, Sidje RB. Stochastic chemical kinetics and the total quasi-steady-state assumption: Application to the stochastic simulation algorithm and chemical master equation. J Chem Phys. 2008; 129(9):095105. https://doi.org/10.1063/1.2971036 PMID: 19044893

61. Kim JK, Josić K, Bennett MR. The Validity of Quasi-Steady-State Approximations in Discrete Stochastic Simulations. Biophys J. 2014; 107(3):783–793. https://doi.org/10.1016/j.bpj.2014.06.012 PMID: 25099817

62. Kim JK, Josić K, Bennett MR. The relationship between stochastic and deterministic quasi-steady state approximations. BMC Syst Biol. 2015; 9:1–13. https://doi.org/10.1186/s12918-015-0218-3 PMID: 26597159

63. Kim JK, Sontag ED. Reduction of multiscale stochastic biochemical reaction networks using exact moment derivation. PLoS Comput Biol. 2017; 13(6):1–24. https://doi.org/10.1371/journal.pcbi.1005571 PMID: 28582397

64. Herath N, Del Vecchio D. Reduced linear noise approximation for biochemical reaction networks with time-scale separation: The stochastic tQSSA+. The Journal of Chemical Physics. 2018; 148 (9):094108. https://doi.org/10.1063/1.5012752

65. Jithinraj PK, Roy U, Gopalakrishnan M. Zero-order ultrasensitivity: A study of criticality and fluctuations under the total quasi-steady state approximation in the linear noise regime. Journal of Theoretical Biology. 2014; 344:1–11. https://doi.org/10.1016/j.jtbi.2013.11.014 PMID: 24309434

66. Chae SJ, Kim DW, Lee S, Kim JK. Spatially coordinated collective phosphorylation filters spatiotemporal noises for precise circadian timekeeping. iScience. 2023; 26(4):106554. https://doi.org/10.1016/j.isci.2023.106554 PMID: 37123226

67. Jeong EM, Kim JK. A robust ultrasensitive transcriptional switch in noisy cellular environments. npj Systems Biology and Applications. 2024; 10(1):30. https://doi.org/10.1038/s41540-024-00356-2 PMID: 38493227

68. Song YM, Campbell S, Shiau L, Kim JK, Ott W. Noisy Delay Denoises Biochemical Oscillators. Phys Rev Lett. 2024; 132:078402. https://doi.org/10.1103/PhysRevLett.132.078402 PMID: 38427894

69. Song YM, Hong H, Kim JK. Universally valid reduction of multiscale stochastic biochemical systems using simple non-elementary propensities. PLoS Comput Biol. 2021; 17(10):1–21. https://doi.org/10.1371/journal.pcbi.1008952

70. MacNamara S, Strang G. Operator splitting. In: Glowinski R, Osher SJ, Yin W, editors. Splitting methods in communication, imaging, science, and engineering. Springer; 2016. p. 95–114.